Enhancing Floating Breakwater and Wave Energy Converter Performance Using Local Resonators

Agarwal, S.[1], Liang, C.[1], Faragau, A.[1] and Colomés, O.[1,*]

[1] Faculty of Civil Engineering and Geosciences, Delft University of Technology, Delft, The Netherlands

Abstract. This paper presents a floating membrane equipped with local resonators as a dual-function system for wave energy harvesting and wave attenuation. Conventional floating breakwaters need to be very long to interact with long, low-frequency ocean waves, where most of the ocean's energy is concentrated. This concept uses a resonator to achieve the same effect, thereby, removing the need for a long floating breakwater. A coupled membrane–fluid–resonator model is developed to study the effect of the resonators on the wet natural frequencies, modal interaction, and wave reflection/transmission. The results show that properly tuned resonators can increase energy absorption at low frequencies while simultaneously reducing transmitted wave amplitude. The proposed system demonstrates how locally resonant concepts can be translated to hydroelastic structures to combine coastal protection and renewable energy harvesting within a single platform.

Key words: *Hydroelastic metamaterials; Wave energy harvesting; Floating breakwaters; Locally resonant metamaterials*

1. Introduction

Coastal regions are increasingly exposed to rising sea levels and intensifying wave climates, while simultaneously being identified as prime locations for large-scale renewable energy extraction. This dual pressure calls for infrastructure that does not merely resist wave action, but interacts with it in a productive manner. Conventional floating breakwaters are designed to attenuate wave energy through reflection and dissipation, whereas wave energy converters aim to maximize energy capture, often as standalone devices. These approaches are typically treated separately, leading either to passive protection systems or to energy harvesters with limited coastal shielding. Bridging this divide requires structural concepts that simultaneously attenuate incident waves and convert their energy into usable power.

Hydroelastic structures provide a promising framework for such multi-functionality [1]. Unlike rigid barriers, floating flexible membranes deform under wave loading, enabling distributed interaction with the wave field over an extended footprint. If appropriately engineered, this deformation can be exploited to both reduce transmitted wave energy and activate energy conversion mechanisms integrated with the structure [2]. The challenge arises from the requirement that a floating breakwater must be comparable in length to the wavelength of the waves it interacts with. Low-frequency ocean waves, which carry most of the ocean's energy, can have very long wavelengths, making the required structure impractically large. Therefore, the objective of this work is to enable the interaction of floating flexible structures with low-frequency ocean waves, without the need for impractically large structures.

Recent advances in metamaterials offer a pathway toward this objective. Metamaterials were first developed in electro-magnetics to achieve unconventional wave manipulation through engineered sub-wavelength structures. Shortly thereafter, the concept of locally resonant inclusions was translated to acoustics and elastodynamics, where subwavelength bandgaps were demonstrated using internal resonators [3]. In mechanical and structural systems, such locally resonant elements have since been

[*]Correspondence to: j.o.colomesgene@tudelft.nl

exploited for vibration suppression [4], band-gap formation [5], and enhanced energy harvesting by concentrating wave energy into discrete oscillators [6]. Early demonstrations showed that metamaterial-inspired wave focusing and localization can dramatically amplify piezoelectric harvesting from structure-borne waves [7]. Subsequent metastructure concepts combining distributed resonators with piezoelectric elements further established the dual functionality of attenuation and energy extraction [8, 9]. Translating these concepts to hydroelastic floating systems enables frequency-selective amplification of membrane deformation, thereby improving harvesting efficiency while simultaneously inducing wave attenuation through resonant energy trapping mechanisms.

In this paper, we investigate a floating membrane equipped with one row of local resonators as a dual-function system that acts both as a wave-energy harvester and as a floating breakwater, see sketch in Figure 1. The analysis focuses on the coupled hydroelastic dynamics and on the role of the resonator in modifying the system's natural frequencies, modal interactions, and energy dissipation characteristics. Through this framework, we assess the potential of resonator-enhanced hydroelastic structures to provide integrated coastal protection and renewable energy extraction within a single scalable platform.

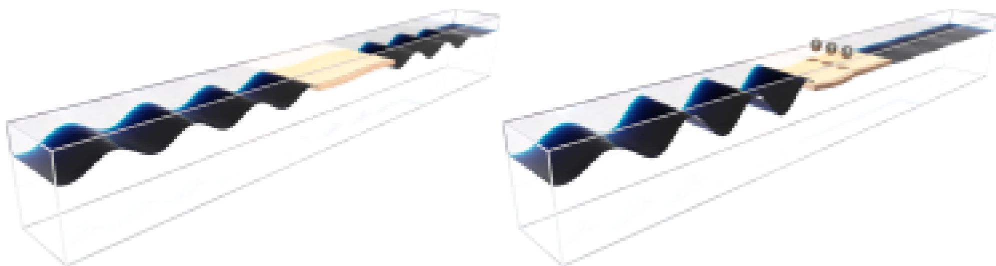

Figure 1: Sketch of the response of a floating flexible membrane under regular waves (left), and response of a floating flexible membrane with a row of resonators (right).

2. Problem setting

In this work we consider a floating flexible structure with negligible bending stiffness, i.e. floating membrane, with a row of resonators mounted on top. The resonators are represented as point masses attached to the structure through a linear spring and linear damper. At its turn, the structure is floating in fluid domain, denoted as Ω. The fluid domain is bounded by inlet and outlet surfaces, Γ_{in} and Γ_{out}, respectively, an irregular bottom surface, Γ_{b}, fluid free-surface, Γ_{fs}, and thin flexible structure (membrane) surface, Γ_{m}. Note that the upper boundary of the fluid domain is composed by the union of free-surface and structure surface, $\Gamma_{\text{fs}} \cup \Gamma_{\text{m}}$, and that the intersection of the free-surface and structure surface define the boundary of the structure, denoted by Λ_{m}, i.e. $\Lambda_{\text{m}} = \Gamma_{\text{fs}} \cap \Gamma_{\text{m}}$. In Figure 2 we depict a sketch of a 2D section of the floating hydroelastic structure with a mounted resonator where all these domains are defined.

We assume the fluid to be incompressible and inviscid and the flow to be irrotational, which enables a unique definition of the flow by means of the velocity potential. We also assume that free-surface wave amplitudes are small compared to the wave-length and water-depth. In that case, the fluid motion can be described via linearised potential flow theory. Furthermore, we assume that there is no separation between floating structure and fluid, thus, the deflection of a structure with negligible draft is equal to the free-surface elevation in Γ_{fs}. For the sake of simplicity we consider homogeneous structural properties, but the same formulation could be used for inhomogenous, i.e. space-dependent, material properties, see [10]. In this work we do not consider nonlinear waves nor nonlinear structural deformations.

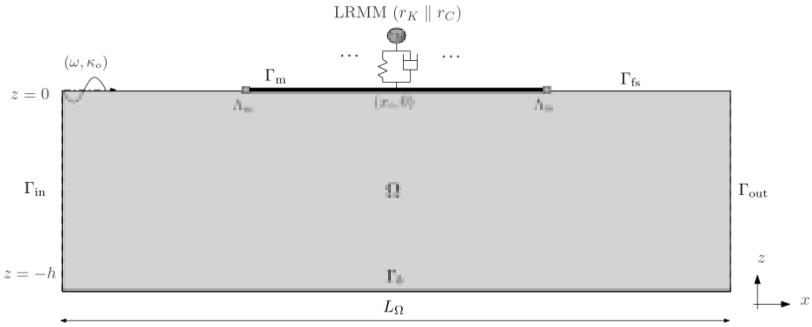

Figure 2: Schematic of the 2D computational domain of the floating hydroelastic structure with attached local resonators.

2.1. Governing equations

Let us consider a scalar velocity potential field, ϕ, defined in the fluid domain, Ω, such that the fluid velocity can be defined as $\mathbf{u} = \nabla\phi$. The fluid is assumed to be incompressible, i.e. $\nabla \cdot \mathbf{u} = 0$, leading to the potential flow governing equation

$$\Delta\phi = 0 \qquad \text{in } \Omega. \tag{1}$$

The governing equation of the fluid is supplemented by appropriate kinematic boundary conditions.

$$\mathbf{n} \cdot \nabla\phi = 0 \text{ on } \Gamma_{\text{b}}, \tag{2a}$$
$$\mathbf{n} \cdot \nabla\phi = u_{\text{in}} \text{ on } \Gamma_{\text{in}}, \tag{2b}$$
$$\mathbf{n} \cdot \nabla\phi = u_{\text{out}} \text{ on } \Gamma_{\text{out}}, \tag{2c}$$
$$\mathbf{n} \cdot \nabla\phi = \kappa_t \text{ on } \Gamma_{\text{fs}}, \tag{2d}$$
$$\mathbf{n} \cdot \nabla\phi = \eta_t \text{ on } \Gamma_{\text{m}}. \tag{2e}$$

In (2), $\mathbf{n}$ is the outward normal to the domain boundary, u_{in} is the velocity component normal to the inlet boundary, u_{out} is the velocity component normal to the outlet boundary, κ_t is the time derivative of the free-surface elevation and η_t is the time derivative of the structure deflection. From the linearized Bernoulli equation, we can relate pressure with free-surface elevation and velocity potential.

$$p = -\rho\phi_t - \rho g\kappa, \qquad \text{on } \Gamma_{\text{fs}}, \qquad p = -\rho\phi_t - \rho g\eta, \qquad \text{on } \Gamma_{\text{m}}. \tag{3}$$

Where ρ is the fluid density and g the gravitational acceleration. We assume that the pressure at the free-surface Γ_{fs} is equal to the atmospheric pressure, which is considered zero in this work. Then, the dynamic boundary condition at the free-surface reads

$$\phi_t = -g\kappa, \qquad \text{on } \Gamma_{\text{fs}}. \tag{4}$$

Let us consider a resonator of mass r_M, attached to the flexible structure with a spring of elastic constant r_K and a damper with damping coefficient r_C, see Figure 2. In this study we consider a pre-tensioned viscoelastic membrane with uniform tension per unit width $T\,(N/m)$, uniform mass per unit length $m\,(kg/m)$ (or unit area in the case of 3 dimensions) and uniform viscous damping parameter τ. The deflection of the membrane coupled with an elastically mounted resonator is given by the governing equations

$$m\eta_{tt} - \nabla \cdot (T\,(\nabla\eta + \tau\nabla\eta_t)) + (r_K(\eta - \xi) + r_C(\eta_t - \xi_t))\,\delta(\mathbf{x}_r) = p, \qquad \text{on } \Gamma_{\text{m}}, \tag{5a}$$
$$r_M\xi_{tt} + r_C\,(\xi_t - \eta_t(\mathbf{x}_r)) + r_K\,(\xi - \eta(\mathbf{x}_r)) = 0. \tag{5b}$$

In equation (5a), η_{tt} is the second derivative with respect to time of the membrane deflection, i.e. acceleration. The variable ξ is the vertical displacement of the resonator, and ξ_t and ξ_{tt} the respective velocity and acceleration. Also in equation (5a), we use $\delta(\mathbf{x}_r)$ to denote the Dirac delta function evaluated at the membrane location, $\mathbf{x}_r$, where the resonator is attached. The governing equation of the membrane should be supplemented with appropriate boundary conditions. Here we assume that the structure boundaries are free, that is

$$T\left(\nabla\eta + \tau\nabla\eta_t\right)\cdot\mathbf{n} = 0 \qquad \text{on } \Lambda_{\mathrm{m}}. \tag{6}$$

Note that the pressure felt by the fluid in equation (3) has to be equal to the pressure felt by the structure in equation (5a). Therefore, we can merge the two equations, resulting into a modified dynamic boundary condition for the fluid at Γ_{m} given by

$$r_{M,\rho}\eta_{tt} - \nabla\cdot\left(T_\rho\left(\nabla\eta + \tau\nabla\eta_t\right)\right) + \left(r_{K,\rho}(\eta-\xi) + r_{C,\rho}(\eta_t - \xi_t)\right)\delta(\mathbf{x}_r) + \phi_t + g\eta = 0, \qquad \text{on } \Gamma_{\mathrm{m}}. \tag{7}$$

Where the subscript $(\cdot)_\rho$ denotes quantities normalized by the fluid density, e.g. $r_{M,\rho} = r_M/\rho$.

Therefore, the dynamic behaviour of locally resonant hydroelastic structures is governed by the set of coupled equations (1, 4, 7 and 5b), which can be used to determine the system variables $\{\phi, \kappa, \eta, \xi\}$, with boundary conditions defined by equations (2) and (6) .

Since we have a linear system, using separation of variables, for a problem with regular waves of frequency ω we can express the system unknowns as $s(\mathbf{x}, t) = \bar{s}(\mathbf{x})\exp(-\imath\omega t)$, for $s = \phi, \kappa, \eta, \xi$. Where the variable $\bar{s}$ represents the space-dependent amplitudes of the velocity potential, free-surface elevation, structure deflection and resonators vertical motion, respectively. For the sake of simplicity, hereinafter we will neglect the over-bar notation and assume that, in the frequency domain context, the variables ϕ, κ, η and ξ will refer to solution amplitudes.

2.2. Numerical Formulation

In this section we describe the numerical formulation based on a finite element approximation of the coupled fluid-structure-resonators problem. We use the finite element method with a monolithic formulation, i.e. solving a unique fully coupled system, extending the formulation firstly proposed for the hydroelastic analysis of floating beams and plates in [11] and later extended to membranes in [12]. Here we first derive the continuous weak form of the problem, followed by the discrete version.

Let us define the inner product between two functions defined in Ω as $(u, v) = \int_\Omega u(\mathbf{x})v(\mathbf{x})\, d\Omega$.Let $\mathcal{V}$ be a suitable functional space in Ω, $\mathcal{V}_{\Gamma_{\mathrm{fs}}}$ the trace space of $\mathcal{V}$ on the free surface Γ_{fs} and $\mathcal{V}_{\Gamma_{\mathrm{m}}}$ the trace space of $\mathcal{V}$ on the structure Γ_{m}, *i.e.* $\mathcal{V}_{\Gamma_{\mathrm{fs}}} = \{v|_{\Gamma_{\mathrm{fs}}} : v \in \mathcal{V}\}$ and $\mathcal{V}_{\Gamma_{\mathrm{m}}} = \{v|_{\Gamma_{\mathrm{m}}} : v \in \mathcal{V}\}$, respectively. We define the velocity potential $\phi \in \mathcal{V}$ and the associated test function $w \in \mathcal{V}$, the free-surface elevation function $\kappa \in \mathcal{V}_{\Gamma_{\mathrm{fs}}}$ and its associated test function $u \in \mathcal{V}_{\Gamma_{\mathrm{fs}}}$ and the membrane deflection $\eta \in \mathcal{V}_{\Gamma_{\mathrm{m}}}$ with associated test function $v \in \mathcal{V}_{\Gamma_{\mathrm{m}}}$. Let us also consider the set of complex numbers $\mathcal{Q} = \mathbb{C}$, containing the value of the resonator motion amplitude and its associated test function, i.e. $\xi \in \mathcal{Q}$ and $q \in \mathcal{Q}$, respectively. Using this notation, the weak form of the problem in the frequency domain, for a given wave frequency ω, reads: *Find* $[\phi, \kappa, \eta, \xi] \in \mathcal{V} \times \mathcal{V}_{\Gamma_{fs}} \times \mathcal{V}_{\Gamma_m} \times \mathcal{Q}$ *such that*:

$$B_\omega([\phi, \kappa, \eta, \xi], [w, v, u, q]) = L_\omega([w, v, u, q]) \qquad \forall[w, v, u, q] \in \mathcal{V} \times \mathcal{V}_{\Gamma_{\mathrm{fs}}} \times \mathcal{V}_{\Gamma_{\mathrm{m}}} \times \mathcal{Q}, \tag{8}$$

with

$$\begin{aligned} B_\omega([\phi, \kappa, \eta, \xi], [w, v, u, q]) = {} & (\nabla\phi, \nabla w)_\Omega + (i\omega\kappa, w)_{\Gamma_{fs}} + (i\omega\eta, w)_{\Gamma_m} + \\ & (-i\omega\phi + g\kappa, \beta(v + \alpha w))_{\Gamma_{fs}} + \\ & (-i\omega\phi + \left(-m_\rho\omega^2 + g\right)\eta, u)_{\Gamma_m} + (T_\rho(1 - i\omega\tau)\nabla\eta, \nabla u)_{\Gamma_m} + \\ & (r_{K,\rho} - i\omega r_{C,\rho})\left(\eta(\mathbf{x}_r) - \xi\right)u(\mathbf{x}_r) + \\ & \left(-r_{M,\rho}\omega^2\xi + (r_{K,\rho} - i\omega r_{C,\rho})\left(\xi - \eta(\mathbf{x}_r)\right)\right)q, \end{aligned} \tag{9}$$

$$L_\omega([w, v, u, q]) = (u_{in}, w)_{\Gamma_{in}} + (u_{out}, w)_{\Gamma_{out}}. \tag{10}$$

The weak form (8) results from standard finite element derivations, we refer the reader to [11, 12] for a detailed explanation of the derivations. Note that the contribution from the resonators results in point-wise evaluations of membrane deflection and corresponding test function, $\eta(\mathbf{x}_r)$ and $u(\mathbf{x}_r)$. The equation of motion of the resonator, equation (5b), is added by testing against the respective test function q, recalling that these is a space-independent scalar complex value.

We use a finite element solver to obtain the solution to the continuous form (8). Here we follow the same approach as proposed in [11, 12, 10], leading to a unique monolithic algebraic system after discretization. Let us consider a triangulation, Ω_h, of the domain Ω, and the corresponding conformal triangulations of the domain boundaries, $\Gamma_{\text{fs,h}}$, $\Gamma_{\text{m,h}}$, $\Gamma_{\text{in,h}}$, $\Gamma_{\text{out,h}}$ and $\Gamma_{\text{b,h}}$. We define the finite-dimensional finite-element spaces for the velocity potential $\mathcal{V}_h$ as follows:

$$\mathcal{V}_h = \left\{ w_h \in \mathcal{C}^0(\Omega) : \; w_h|_K \in \mathbb{P}_r(K), \forall K \in \Omega_h \right\}, \tag{11}$$

and the free surface elevation and membrane elevation, $\mathcal{V}_{\Gamma_{\text{fs}},h}$ and $\mathcal{V}_{\Gamma_{\text{m}},h}$, are the trace spaces of $\mathcal{V}_h$ on the free surface and membrane, respectively. In (11), $\mathbb{P}_r(K)$ is the space of Lagrange polynomials of degree r in an element K, and E are facets of dimension $d-1$, with d being the topological dimension of the domain Ω. In particular we use $r = 2$ in this work. We recall that the space $\mathcal{Q}$ is a finite-dimensional space containing a single complex scalar value.

Using this notation, the final discrete form in the frequency domain reads: *Find* $[\phi_h, \kappa_h, \eta_h, \xi] \in \times \mathcal{V}_{\Gamma_{fs},h} \times \mathcal{V}_{\Gamma_m,h} \times \mathcal{Q}$ *such that for all* $[w_h, v_h, u_h, q] \in \mathcal{V} \times \mathcal{V}_{\Gamma_{fs}} \times \mathcal{V}_{\Gamma_m} \times \mathcal{Q}$:

$$B_\omega([\phi_h, \kappa_h, \eta_h, \xi], [w_h, v_h, u_h, q]) = L_\omega([w_h, v_h, u_h, q]). \tag{12}$$

With B_ω and L_ω as given by equations (9) and (10), respectively.

3. Results

In this section we assess the behaviour of the proposed floating membrane with resonator system. We assume a structure with infinite width, with long-crested regular waves coming in the direction aligned with the structure longitudinal axis. With these assumptions the problem simplifies to a floating 1-dimensional membrane on a 2-dimensional fluid domain. We also assume deep water regime and flat bottom, see sketch in Figure 2.

The length of the membrane is $L_m = 2h$, placed in 2D water domain with depth $h = 10\,(m)$, and length $L_\Omega = 3L_m$. The membrane is made of polyethylene with density of $\rho_s = 922.5(kg/m^3)$ and a thickness of $1m$, thereby resulting in mass per-unit-area of $m = 922.5(kg/m^2)$ and a submerged draft of $0.9(m)$. The membrane is tensioned with a tension per-unit-width $T = 10\rho g$, where $\rho = 1025\,(kg/m^3)$ is the water density. This pre-tensioning can be achieved via floaters, which are not modelled in this analysis. On top of the membrane we place a resonator with variable mass. Otherwise stated, we use a resonator mass of $r_M = 1000\,(kg/m)$ and natural frequency of $2.4\,(rad/s)$. Note that the material properties used in this study might not necessarily lead to a feasible engineering solution, but are selected to highlight the combined effect of hydroelastic structures with local resonators.

3.1. Influence of local resonator on system natural frequencies

As discussed in the introduction, the purpose of the local resonator is to complement the membrane's ability to efficiently harvest energy at specific wave frequencies. As demonstrated in [12], the membrane effectively harvests energy at the natural frequencies of the coupled membrane–fluid system, referred to as the *wet natural frequencies*. Ideally, the local resonator should not significantly alter these wet natural frequencies, but rather enhance the system's performance by enabling efficient energy harvesting at lower frequencies. Accordingly, this section investigates the extent to which the wet natural frequencies are influenced by the addition of the local resonator. For a detailed description of the identification procedure for the wet natural frequencies and their associated mode shapes, the reader is referred to [12].

In particular, we vary the natural frequency $\omega_r = \sqrt{\frac{r_k}{r_M}}$ of the resonator, by varying r_k and keeping a constant mass $r_M = 1000\,(kg/m)$. In Figure 3 we depict how the first 6 natural frequencies of the system, $\omega_n^{(i)}$ with $i = \{0, ..., 5\}$, change when we vary the resonator natural frequency in the range $\omega_r \in [1.0, 5.0]\,(rad/s)$.

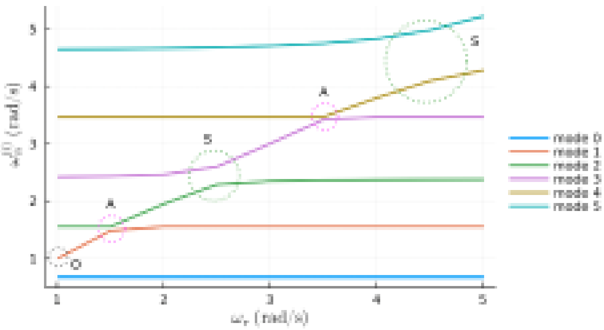

Figure 3: The influence of the natural frequency of the resonator $\omega_r = \sqrt{\frac{r_k}{r_M}}$ on the first 6 natural frequencies of the whole system.

Before discussing the figure, it is important to recall that the resonator is placed at the centre of the membrane and the membrane has two kinds of elastic modes: anti-symmetric (A), where the centre is a node with nearly zero displacement, and symmetric (S), where the centre is an anti-node with significant displacement.

Now coming to Figure 3, consider first the case of $\omega_r = 1$ rad/s. Here we mark 6 natural frequencies of the system $\omega_n^{(i)}$,of which five correspond to the hydroelastic modes of the membrane, while the sixth is governed by the resonator, denoted by marker O. In this configuration, the resonator does not alter the hydroelastic natural frequencies of the membrane.

As we increase ω_r, at some point ω_r approaches one of the hydroelastic natural frequencies of membrane. If the resonator frequency is close a anti-symmetric mode of the membrane, where the centre of the membrane is a node, then the influence of the resonator remains minimal, as seem by markers A. In fact, it appears as if the resonator-dominated mode vanishes. In contrast, when ω_r approaches a symmetric natural frequency, strong modal interaction occurs, as indicated by markers S. This region contains two strongly coupled modes and introduces a band-gap, which may be of interest for exploring meta-material behaviour of this structure.

This result highlights the frequency-selective nature of the coupled system of floating membranes with resonators, which has the ability to inject new modal content into the system close to the resonator natural frequency.

3.2. Response of the undamped system

After assessing the influence of the resonator on the system natural frequencies, we proceed to examine the steady-state dynamic response of the coupled system under monochromatic wave excitation. The incoming wave field is prescribed with a target amplitude $|\kappa_{\text{in}}| = \kappa_0$, assuming linear wave Airy theory, and wave frequency ω. In this section we look into wave reflection, transmission, and absorption coefficients under various incoming wave frequencies without material damping.

Let κ_{in}, κ_{r} and κ_{t} denote the complex-valued wave amplitudes associated with the incident, reflected, and transmitted waves, respectively. With the wave amplitudes we can then compute the corresponding reflection coefficient $K_r = \frac{P_{\text{r}}}{P_{\text{in}}}$ and transmission coefficient $K_t = \frac{P_{\text{total}}}{P_{\text{in}}}$, with the respective power fluxes, P_{in}, P_r, P_t defined as

$$P_{\text{in}} = \frac{1}{2}\rho g|\kappa_{\text{in}}|^2 C_g, \qquad P_{\text{r}} = \frac{1}{2}\rho g|\kappa_{\text{r}}|^2 C_g, \qquad P_{\text{total}} = \frac{1}{2}\rho g|\kappa_{\text{t}}|^2 C_g, \tag{13}$$

with

$$C_g = \frac{1}{2}\frac{\omega}{k}\left(1 + \frac{2kh}{\sinh(2kh)}\right). \tag{14}$$

In equation (14), C_g is the wave group velocity and k the wave number associated to ω, the incoming wave frequency. As a baseline, the dynamic response of the membrane-only configuration is first examined. The computed wet natural frequencies are $\omega^w_{mem} = \{1.553,\ 2.413,\ 3.467,\ 4.642\}$ rad/s, which serve as reference values for interpreting the coupled response. We then consider the undamped coupled system ($\tau = 0$, $r_C = 0$) subjected to a regular wave with $\omega = 2.4$ rad/s, coinciding with ω_r and close to the second wet natural frequency of the membrane.

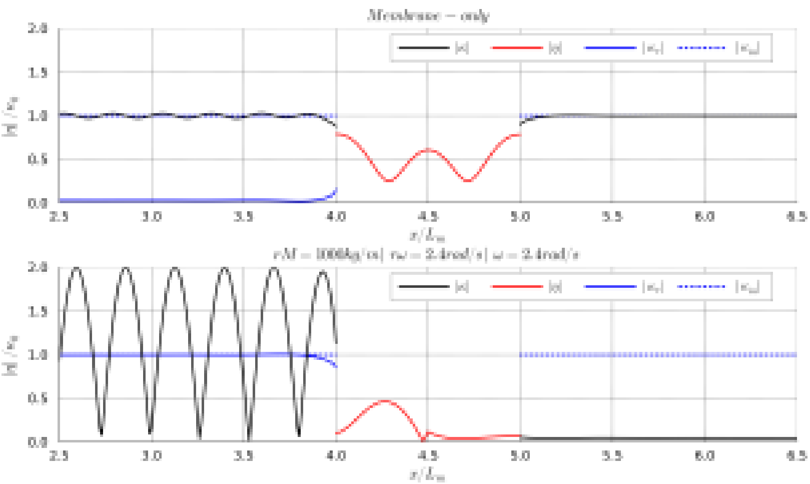

Figure 4: Amplitudes of the structural deflection η, incoming wave κ_{in}, reflected wave κ_r, transmitted wave κ_t, and total free-surface elevation, for an incident wave frequency close to one of the natural frequencies of the membrane-fluid (top) and of the local resonator (bottom).

The spatial amplitudes of the free-surface elevation κ and membrane deflection η are shown in Figure 4, where the upstream field is decomposed into the incident wave κ_{in} and the reflected component $\kappa_r = \kappa - \kappa_{in}$, and the downstream solution represents the transmitted wave $\kappa_t = \kappa$. For the membrane-only case (top Figure. 4), excitation near resonance results in nearly complete transmission with minimal reflection. In contrast, when the resonator frequency coincides with the excitation frequency, strong resonant motion is triggered, leading to almost total reflection and strongly reduced transmission (bottom Figure. 4). This demonstrates that the addition of the resonator enables selective wave-energy capture for frequencies that would otherwise fully transmit through the membrane.

To further investigate the system's dynamic characteristics without material damping, we perform a series of simulations using monochromatic waves with $\omega = [1, 5]$ rad/s, and evaluate the amplitude of the structural response and wave fields at each frequency. The resulting response contours and energy coefficients are shown in Figure 5 and Figure 6.

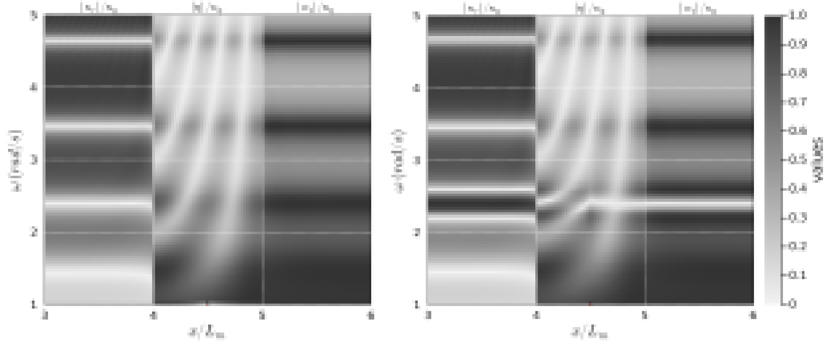

Figure 5: Response contour plots of the normalized amplitude of the deflection η, reflected wave κ_r, and transmitted wave κ_t in the vicinity of the structure for wave frequency $\omega = [1,\ 5]\ rad/s$ for the membrane only (left) and coupled system (right).

Figure 5 compares the membrane-only and coupled responses in terms of the normalized amplitudes of η, κ_r, and κ_t over space and frequency. For the membrane alone, lower frequencies produce larger deflections, whereas higher frequencies yield reduced response, indicating compliance to long waves and relative stiffness to short waves. With the introduction of a local resonator ($\omega_r = 2.4\,\mathrm{rad/s}$), a pronounced amplification of reflected waves emerges near the resonant frequency, demonstrating strong frequency-selective reflection accompanied by a corresponding suppression of the transmitted wave amplitude, while maintaining a structural response comparable to the uncoupled membrane.

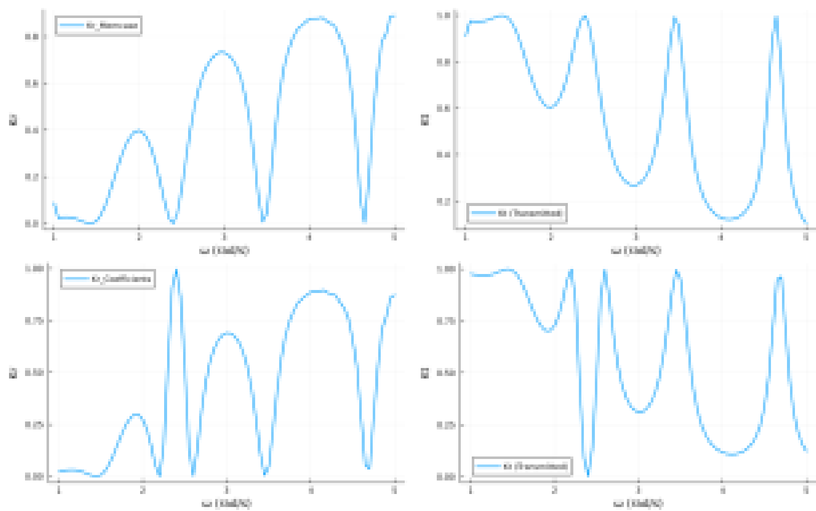

Figure 6: Plots of reflection coefficient K_r (left), transmitted coefficient K_t (right) under monochrome frequency $\omega = [1 : 5]\ rad/s$ for the membrane-only (top) and coupled system (bottom).

This frequency-selective behavior is further quantified by the energy coefficients shown in Figure 6. For the membrane-only system, the structure acts as a frequency-dependent filter: low-frequency waves are largely transmitted, while higher frequencies are reflected. Near the wet natural frequency, K_r exhibits pronounced troughs and K_t corresponding peaks, forming passbands centered around the structural resonance. With the introduction of the resonator, this filtering pattern is fundamentally modified near ω_r. As shown in Figure 6 (bottom row), K_r increases sharply while K_t decreases around the resonator frequency. Extreme flips in K_r and K_t are observed, which reflect the emergence of a bandgap around the resonator frequency.

3.3. Response of the damped system

Having explored the dynamic response of the coupled system in the absence of material damping, we now investigate the influence of resonator damping on the wave–structure interaction. To isolate this effect, the membrane viscoelastic parameter is set to $\tau = 0$ and only internal resonator damping is considered. To characterize the damping within each resonator, we adopt a classical mass-spring-dashpot viscoelastic model, where the damping coefficient r_C is defined through the damping ratio ζ as $r_C = 2\zeta\sqrt{r_K r_M}$. The power dissipated by the resonator damping and the corresponding absorbed wave energy coefficient are defined as

$$P_a = \frac{1}{2} r_C \omega^2 \left|\xi - \kappa\right|^2 , \qquad K_a = \frac{P_a}{P_{in}}. \tag{15}$$

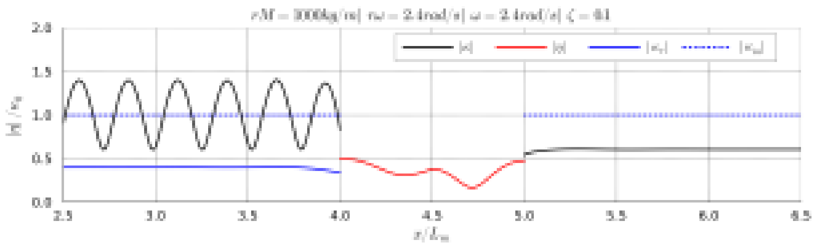

Figure 7: Plot of amplitude of structure deflectionη, incoming wave $\kappa_i n$, reflected wave κ_r, transmitted wave κ_t, and total free-surface elevation for the case with damping ratio $\zeta = 0.1$.

Figure 7 shows the spatial amplitude distribution with resonator damping. We have seen that in the undamped case, see Figure 4 (bottom), the system operates in a nearly fully reflective regime, with negligible transmission. When damping is introduced, the resonant structural amplification is suppressed and the reflected wave amplitude decreases, while transmission increases from nearly zero to a finite level. Since the transmitted wave remains smaller than the incident wave, the redistribution between reflection and transmission is incomplete, indicating that a portion of the incoming energy is dissipated through the resonator damping mechanism. This initial observation suggests that damping can effectively tune the energy partition between reflection and absorption.

Figure 8 shows the normalized amplitudes of η, κ_r, and κ_t for $\zeta = 0.1$ over a range of excitation frequencies. Compared to the undamped configuration result in Figure 5b, the frequency-selective behaviour in Figure 8 becomes less pronounced when resonator damping is introduced. The reflected wave amplitude is lower than in the undamped case, but remains significantly higher than in the membrane-only case. Similarly, the transmission coefficient is higher than in the undamped case, but significantly lower than in the membrane-only case shown in Figure 5a. These observations indicate a redistribution of energy from narrow-band response at the resonator frequency to a wider band response around the resonator frequency, enabled by increased energy dissipation by the resonator.

To further quantify the influence of resonator damping, the frequency domain simulations are repeated for different damping ratios ζ, and the corresponding wave-energy coefficients are computed. The resulting reflection, transmission, and absorption coefficients are shown in Figure 9. As the damp-

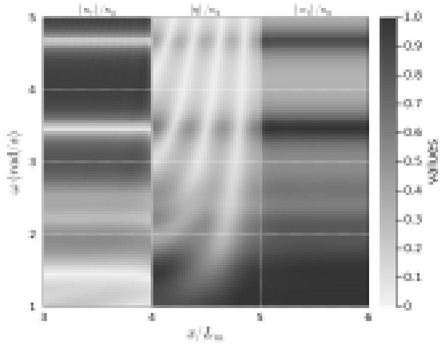

Figure 8: Response contour of coupled system and vicinity water domain with damping ratio $\zeta = 0.1$.

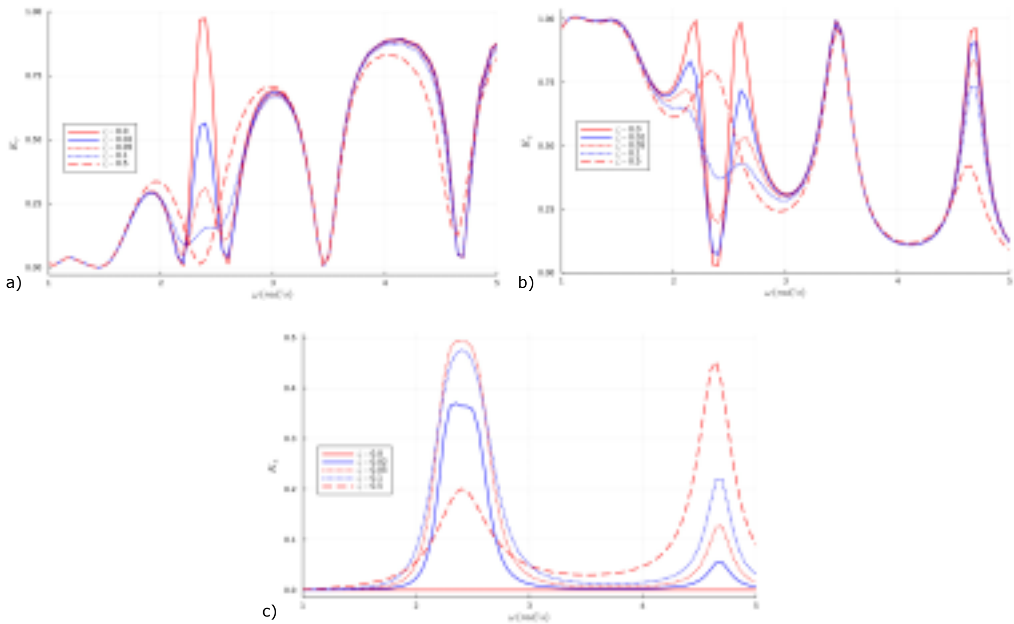

Figure 9: Plots of a) reflection coefficient K_r, b) transmitted coefficient K_t, and c) absorption coefficients K_a for $\zeta = [0.01, 0.02, 0.05, 0.1, 0.5]$ under monochrome frequency $\omega = [1:5]\ rad/s$.

ing ratio increases, a clear redistribution of energy between reflection, transmission, and absorption is observed. For low damping values (e.g., $\zeta = 0.02$), the reflection coefficient K_r near the resonant frequencies remains high, although reduced compared with the undamped case, consistent with the strong wave rejection observed previously. As ζ increases further (e.g., $\zeta = 0.05$ and $\zeta = 0.1$), K_r continues to decrease while the absorption coefficient K_a increases and becomes dominant near resonance, indicating that a significant portion of the incoming wave energy is dissipated by the resonator. The pronounced peaks of K_a around the resonant frequencies confirm the damping-enhanced selective absorption capacity of the system. At very high damping (e.g., $\zeta = 0.5$), the influence of the resonator becomes less pronounced, although K_a remains non-negligible, both K_r and K_t gradually approach the membrane-only behavior.

4. Conclusions

The inclusion of local resonator introduces a strong frequency-dependent energy modulation. The resonator disrupts the original passband structure by creating a localized bandgap around ω_r, where wave reflection is significantly enhanced, showing its potential in reflecting and/or absorbing certain-frequency energy. The addition of damping in the coupled system introduces a tunable mechanism to control both wave reflection and transmission characteristics. Low damping preserves selective filtering with extreme peak–dip transitions in both K_r and K_t around the resonant frequency. Moderate damping smooths this transitions and redistributes energy over broader frequencies. Excessive damping neutralizes local resonator's effects, rendering the system nearly equivalent to the baseline membrane. These findings highlight the critical sensitivity of wave-structure interactions to the damping level and offer practical insights for engineering resonator-based coastal or floating systems.

Acknowledgments

This publication is part of the project "Hydroelastic Black Holes for Offshore Renewable Energy" with file number OCENW.XS24.2.127 of the research programme ENW-XS which is financed by the Dutch Research Council (NWO).

References

[1] Miguel Lamas-Pardo, Gregorio Iglesias, and Luis Carral. A review of very large floating structures (vlfs) for coastal and offshore uses. *Ocean Engineering*, 109:677–690, 2015.

[2] XL Zhao, DZ Ning, QP Zou, DS Qiao, and SQ Cai. Hybrid floating breakwater-wec system: A review. *Ocean engineering*, 186:106126, 2019.

[3] Z. Liu, X. Zhang, Y. Mao, Y. Y. Zhu, Z. Yang, C. T. Chan, and P. Sheng. Locally resonant sonic materials. *Science*, 289(5485):1734–1736, 2000.

[4] G. L. Huang and C. T. Sun. Band gaps in a multiresonator acoustic metamaterial. *Journal of Vibration and Acoustics*, 131(3):031003, 2009.

[5] Y. Xiao, J. Wen, and X. Wen. Flexural wave band gaps in locally resonant beams with periodically attached resonators. *Journal of Physics D: Applied Physics*, 45(19):195401, 2012.

[6] M. Carrara, M. R. Cacan, M. J. Leamy, M. Ruzzene, and A. Erturk. Dramatic enhancement of structure-borne wave energy harvesting using an elliptical acoustic mirror. *Applied Physics Letters*, 100(20):204105, 2012.

[7] M. Carrara, M. Ruzzene, and A. Erturk. Metamaterial-inspired structures and concepts for elastoacoustic wave energy harvesting. *Smart Materials and Structures*, 22(6):065004, 2013.

[8] G. Hu, L. Tang, A. Banerjee, and R. Das. Metastructure with piezoelectric element for simultaneous vibration suppression and energy harvesting. *Journal of Vibration and Acoustics*, 139(1):011012, 2017.

[9] J. Li, X. Zhou, G. Huang, and G. Hu. Acoustic metamaterials capable of both sound insulation and energy harvesting. *Smart Materials and Structures*, 25(4):045013, 2016.

[10] Kareem El Sayed, Shagun Agarwal, Andrei Metrikine, and Oriol Colomés. Adjoint-based PDE-constrained optimization of viscoelastic floating membrane for maximum wave power absorption. *Structural and Multidisciplinary Optimization*, 69(3):71, February 2026.

[11] Oriol Colomés, Francesc Verdugo, and Ido Akkerman. A monolithic finite element formulation for the hydroelastic analysis of very large floating structures. *International Journal for Numerical Methods in Engineering*, 124(3):714–751, 2023.

[12] Shagun Agarwal, Oriol Colomés, and Andrei V Metrikine. Dynamic analysis of viscoelastic floating membranes using monolithic finite element method. *Journal of Fluids and Structures*, 129:104167, 2024.